Carbon Monoxide Measurements in an Inductively Coupled CO_2 Plasma Using Two-Photon Laser Induced Fluorescence

B. J. Voll* J. C. Schindler* R. Herrmann-Stanzel† J. M. Meyers‡, and D. G. Fletcher§
University of Vermont, Burlington, VT

Uncertainties in surface catalytic reaction rates in a CO_2 plasma has led to over-design of thermal protection systems which has caused atmospheric entry vehicles for the Martian atmosphere to be heavier than necessary and therefore decreased the available payload of various missions. A better understanding of these reaction rates will allow for more precise development of thermal protection systems leading to safer and more effective atmospheric entry vehicles. Near wall measurements in a plasma facility using laser spectroscopic techniques with sub-millimeter spatial resolution provides a method to determine surface-catalyzed reaction efficiency measurements over a cooled copper surface. This work provides laser induced fluorescence measurements of oxygen atoms and carbon monoxide molecules in a predominantly CO_2 plasma produced by inductive coupling. These measurements are used to determine temperature, relative number density, surface-catalyzed reaction rates and catalytic efficiencies for CO_2 recombination and O_2 recombination. Catalytic recombination efficiency values of 0.0274 ± 0.0090 for recombination of O_2 and 0 ± 0.0004 for recombination of CO_2 suggest that molecular oxygen recombination is the dominant reaction and that a super-catalytic boundary condition is overly-conservative.

I. Introduction

AERO-THERMODYNAMIC heating is one of the most important considerations when designing atmospheric entry vehicles and their corresponding Thermal Protection System (TPS) [1]. The TPS makes up a large portion of the mass of the vehicle, thereby making it a priority to minimize the weight of the TPS to allow a maximum payload to be delivered. At sufficiently high speeds, a shock layer forms ahead of the vehicle where the quiescent equilibrium atmospheric gases dissociate into a mixture of molecules and atoms. In the post shock region, if the pressure is sufficiently high and the temperature is sufficiently low, recombination of these constituent components may occur. Depending on the surface material of the entry vehicle and its catalycity, further exothermic recombination can occur causing additional heating to the surface of the vehicle. Design of Thermal Protection Systems takes a conservative approach when calculating the expected thermal load the vehicle will encounter [2–4]. There is a particular uncertainty in the surface catalyzed recombination reactions in a predominantly CO_2 plasma [5]. A better understanding of these reactions will allow for development of reduced TPS mass and more payload availability.

The Martian atmosphere is made up of approximately 95% CO_2, 2.6% N_2, 1.9% Ar, and trace amounts of O_2 and CO. Equilibrium conditions, calculated using CEA [6] and seen in Fig. 1 , shows the evolution of the CO_2 gas at a constant pressure and varying temperature, which corresponds to conditions experienced in the University of Vermont (UVM) 30 kW Inductively Coupled Plasma (ICP) Torch Facility. Argon is added as a buffer gas to aid in the development of the plasma but does not contribute to surface reactions as it is an inert gas. Plasma is generated at about 10,000 K in the induction zone, creating a plasma ball. The plasma is ejected into the chamber as a free jet where the temperature corresponds to a large amount of dissociated O and CO. With further cooling, as the distance to the sample surface decreases, the O and CO molecules begin to recombine into other forms which may or may not be the original gas chemistry. The rate at which this recombination occurs is dependent on the catalycity of the sample surface if a sample is inserted in the flow.

There are three cases when discussing catalycity. The first is super-catalytic. This is when all the available chemical energy in the boundary layer is deposited on the surface. The fully-catalytic case recombines to equilibrium at the surface. The non-catalytic case produces low heating rates and minimal recombination on the surface. When making

*Graduate Research Assistant, Department of Mechanical Engineering
†PhD Candidate, Department of Mechanical Engineering
‡Research Assistant Professor, Department of Mechanical Engineering and AIAA Senior Member
§Professor, Department of Mechanical Engineering and AIAA Associate Fellow

conservative design choices, typically a super or fully-catalytic model is used. Even a fully-catalytic model can produce twice the heat flux as a non-catalytic model at hypersonic speeds [7]. When using these higher catalytic cases, heat shields are designed to be heavier and more robust than likely necessary, diminishing the available payload for the mission.

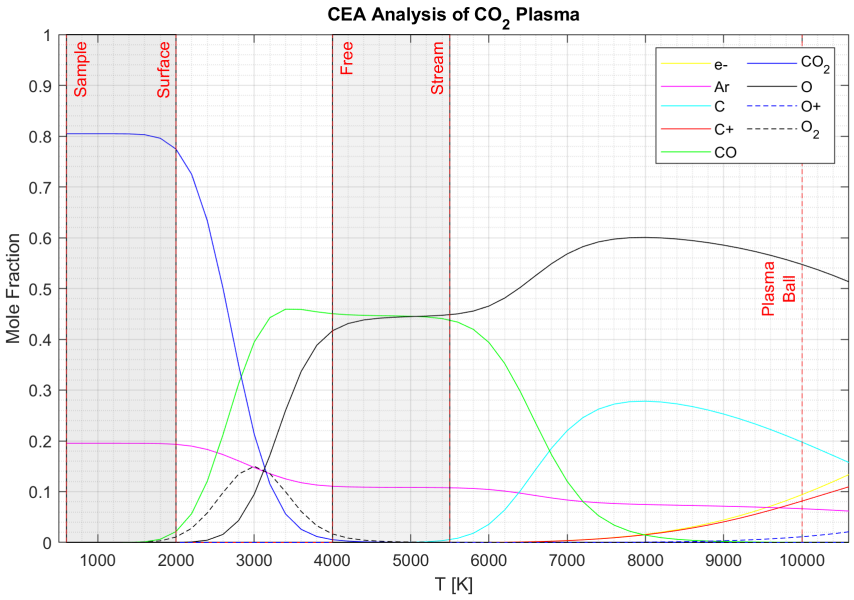

Fig. 1 Mars Equilibrium Chemistry with Argon Buffer at 160 Torr Calculated Using CEA.

Chen [8] first developed a rate model and determined that surface catalysis was an important parameter to consider. A catalysis model was soon developed for the Mars Pathfinder Program by Mitcheltree [9] consisting of the following reactions:

$$O + (s) \rightarrow O_s \quad ; \quad CO + O_s \rightarrow CO_2$$

$$CO + (s) \rightarrow CO_s \quad ; \quad O + CO_s \rightarrow CO_2 \tag{1}$$

In this model, it is assumed that recombination to CO_2 is the predominant reaction and that a super-catalytic condition takes place. It is already noted why a super-catalytic assumption is unfavorable, but it is also important that a substantial reaction is neglected in this model. The atomic to molecular oxygen recombination reaction, seen in Eq. 2, is neglected.

$$O + O \rightarrow O_2 \tag{2}$$

Sepka used two photon laser induced fluorescence on quartz in a diffusion tube side-arm reactor to probe O and CO to determine how dominant CO and oxygen recombination are. The findings from this study were that the presence of CO in the gas phase does not significantly affect the oxygen recombination reaction on quartz and gas-phase CO concentration is not significantly altered by atomic oxygen [10]. These results suggest that atomic to molecular oxygen recombination is the dominant reaction, contrary to the Mitcheltree model and suggesting that a super-catalytic model is an unlikely case.

Further testing done in an inductive plasmatron by Kolesnikov held the view that only homogeneous catalytic reactions, such as the O_2 reaction, are possible in a dissociated CO_2 gas mixture [11].

The Mars Science Laboratory (MSL) Program launched in 2011 with an on-board suite of instrumentation to develop entry descent and landing design. Studies needed to be done to determine the design of the heat shield to be used on the mission. MacLean [12, 13] utilized the LENS shock tunnel at CUBRC and Wright [14] utilized the T5 shock tunnel at GALCIT to compare with numerical simulations of test cases. It was found that the heat fluxes of the

facilities only matched the numerical simulations if a super-catalytic condition was used. This contradicts the previous findings by Sepka where it was determined that a super-catalytic model was unnecessary.

Soon after these findings Marschall [15] found that oxygen molecule recombination was partially catalytic and that the CO_2 reaction was non-catalytic using a side-arm reactor on varying metallic samples. This agrees with Sepka's findings and disagrees with MacLean and Wright. Gnoffo concluded that an assumption can be made that either the O_2 reaction or the CO_2 reaction can be used in the Martian atmosphere as long it is fully-catalytic [16].

With these findings and the uncertainty between the two competing theories, the conservative approach of a super-catalytic boundary condition was used in the design of MSL as this was the safer approach and was at the time accepted as the normal [17].

An new facility at CUBRC known as the LENS-XX provided further testing for an extensive database of heating, pressure, and flowfield measurements in high-enthalpy carbon-dioxide flows. Fully-catalytic and non-catalytic simulations were used to bound the experimental data as it is noted that prior uncertainty in catalytic recombination heating is high. The uncertainty in the prior results has resulted in previous testing to be considered invalid. The bound between non-catalytic and super-catalytic is imposed only on the homogeneous atomic recombination of O_2, and all other reactions, such as Eq. 1, are considered to be non-catalytic. Results showed that the data was typically bounded between the fully-catalytic and non-catalytic simulations and also trended towards the non-catalytic bound [18, 19]. It is of note that previous testing from this facility, [12, 13], found that only a super-catalytic model agreed with experimental heat flux results. This shows a reversal and data seems to be trending towards a more accepted semi-catalytic boundary condition that agrees with the Sepka and Marschall findings. Continuing to unravel these past contradictions will prove to be useful to future Martian missions as TPS can be designed less conservatively and allow for higher payloads.

Objectives and Methods

The objective of this work is to better understand surface catalyzed recombination reactions in a CO_2 plasma on a copper surface, so as to further the understanding of the reactions and reduce the uncertainty described above. The UVM ICP Facility will be utilized to create the conditions necessary for this study. Probing of oxygen atoms using two-photon absorption laser induced fluorescence (TALIF) is an already proven method used in the lab, and a new approach to probing CO will be developed that can be used in conjunction with oxygen atom measurements to determine temperature and number density measurements. With these techniques the recombination efficiency can be determined for both O_2 and CO recombination.

The following sections present the UVM ICP Facility, the test conditions used in this investigation, and the laser diagnostic methods employed for testing. The theoretical approach follows with a discussion on previous results and than current results of measurements taken over a water-cooled copper sample. A summary is given to conclude as well as planned future work.

II. UVM Inductively Coupled Plasma Facility Description

The University of Vermont houses a 30 kW ICP Facility. This facility allows for the testing of advanced aerospace materials through means of replicating the conditions experienced through atmospheric re-entry. The US more typically houses arc-heated facilities for similar investigations. Arc-heaters produce contaminated flow because the arc is attached to electrodes which produce molten copper that is entrained in the flow. ICP facilities match the heat flux experienced by the object as well as the physical environment through plasma generation. The method by which the plasma generation occurs is through an induced RF magnetic field created by a helical load coil. The load coil surrounds a quartz tube which sits upon an injector-block assembly. This is shown in Fig. 2. The 30 kW power supply creates an induced magnetic field through the RF coils. The magnetic field oscillates at a known frequency and couples with the injected gas which dissociates and ionizes the present gases thereby creating a plasma [20]. This provides a contaminant free flow as there are no electrodes in the flow. Because of this spectroscopic measurements are more suitable in an ICP facility than an arc facility. A benefit of arc-heated facilities is that they can cover a wide pressure range therefore making them able to cover a wide range of flight-trajectories. ICP facilities are operated at or lower than atmospheric pressures.

The 30 kW power supply is a Lepel Model T-30-3-MC5-J-TL1 induction heating generator that operates at a frequency between 2.5-5 MHz and is checked periodically with a bnc loop. Operation for this work is near 2.5 MHz. It provides high output DC power which is converted to the RF field [20]. After the plasma is created it exits the quarts tube vertically into a vacuum chamber as a free jet. The vacuum chamber is made of stainless steel to avoid contaminants and is water cooled due to the high heat that the plasma generates. It also has multiple ports which allow for a variety of sample holders (known as probes) as well as viewing windows which are used for spectroscopic measurements, laser

diagnostics, temperature measurements, etc.. A vacuum pump exhausts the gases in the chamber which are initially supplied by high pressure tanks. Mass flow controllers restrict the flow from the high pressure tanks and allow for a steady, known gas supply. These components are shown in Fig. 2.

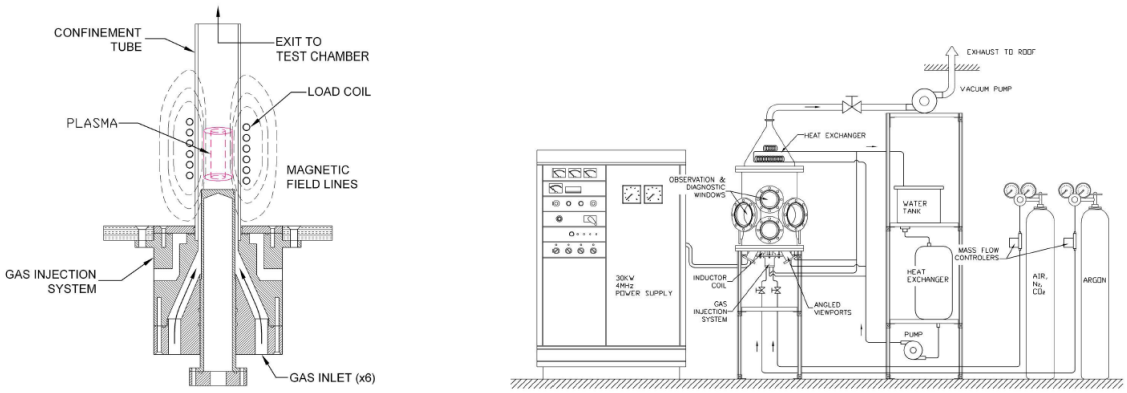

(a) **(b)**

Fig. 2 a) Gas Injection Schematic. b) Schematic portraying the UVM ICP Torch facility.

The facility is able to replicate a variety of different conditions with various gas mixtures. An overview of the conditions which can be achieved in the facility are shown in Table 1.

Table 1 University of Vermont Inductively Coupled Plasma Torch Specifications.

Parameter	Specification	This Work
Test Gas	Air, Ar, N_2, O_2, CO_2	CO_2, Ar
Power	30 kW @ 2-3 MHz	30 kW @ 2.5 MHz
Heat Flux	10-100 W/cm^2	10-100 W/cm^2
Enthalpy	5-20 MJ/kg	2-10 MJ/kg
Mach	$<$0.3 & $>$1.0	$\sim$0.3
Test Pressure	100-200 Torr	160 Torr
Run Time	$>$1 hr	$>$1 hr

The goal of the facility is to replicate the conditions experienced at hypersonic speeds in various atmospheric conditions. This is done by matching boundary-layer edge velocity gradient, enthalpy, and total pressure of a flight-trajectory for a given atmospheric composition [21]. At hypersonic speeds, a detached bow shock will form in front of a blunt body such as a re-entry vehicle, as seen in Fig. 3a. Behind the shock wave the flow is subsonic. The slowing of the flow and increase in pressure causes a large increase in temperature behind the shock. Added to this is the increase in temperature at the surface of the vehicle caused by friction from the surrounding atmosphere. CO_2 begins to dissociate at about 2400 K and most of the molecules are dissociated by 4000 K according to a Gibbs free energy analysis [22].

In the UVM ICP torch, the plasma exits the quartz tube vertically and moves upwards in the chamber. As the plasma moves away from the exit, it slowly begins to expand outwards and cool, evolving toward a local thermodynamic equilibrium (LTE) state. Using mass flow controllers to limit the amount of gas that is injected into the chamber, and a PID to control the pressure within the chamber, the plasma flow remains laminar which is necessary to obtain reliable results. By the time the plasma reaches the surface of a sample, it has cooled sufficiently to produce similar conditions to those experienced by entry vehicles in the Martian atmosphere. A view of the sample is shown in Fig. 3b. A small boundary layer forms above the surface of the sample just as on a flight vehicle. Measurements can be taken at this location to determine the chemical reactions and the rates they are occurring. The samples used have a geometry with a body diameter of 25.4 mm, a leading edge corner radius of 3.2 mm, and a depth of 12.7 mm. The samples are mounted on a probe which holds the sample perpendicular to the flow in a stagnation-point configuration.

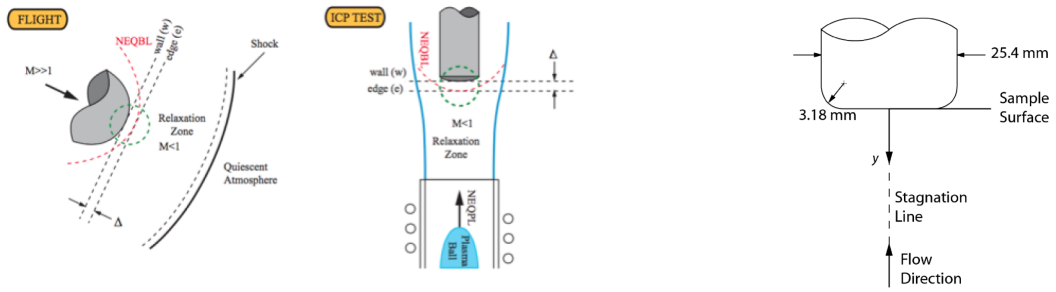

(a) **(b)**

Fig. 3 a) Comparison between in flight conditions and the UVM ICP facility. b) Schematic portraying water-cooled copper sample with key dimensions.

III. Two Photon Absorption Laser Induced Fluorescence of O and CO

Two photon laser induced fluorescence is the main method used for determining temperature and number density measurements. It's a spatially resolved, species selective probe of atomic or molecular species. TALIF can probe a specific excitation state of a species using a laser at a precise wavelength which corresponds to the excitation of the species in question. The molecule or atom is excited and spontaneously relaxes back down to a lower energy state. When it relaxes, it emits a photon at a different precise wavelength. This is known as fluorescence. Using specific narrow-bandwidth filters, this emission can be captured whereas blocking other emitted wavelengths. Laser induced fluorescence was first developed by Tango [23] in 1968 and soon after Bamford [24] used TALIF to detect the $3p^3P_{2,1,0} \leftarrow 2p^3P_2$ transition using a Nd:YAG pumped dye laser. Loge and Aldén [25, 26] used a similar setup to excite CO to the $B^1\Sigma^+$ state with 230 nm absorption. These are the same transitions used by the UVM facility. These early experiments had low resolution and improvements in technology over the years have allowed for much higher resolution in the transitions especially for CO [27].

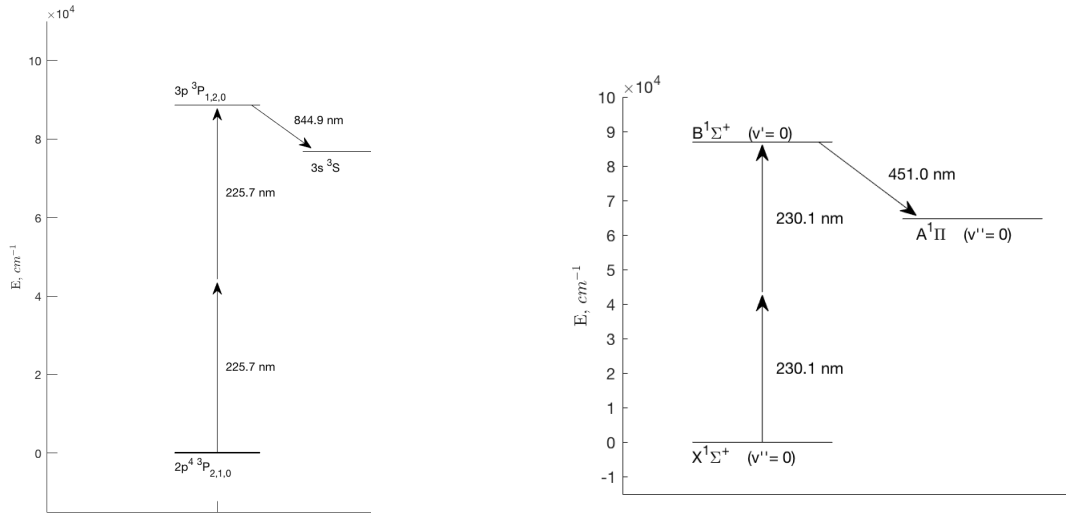

(a) **(b)**

Fig. 4 a) Oxygen atom excitation scheme and energy levels. b) CO excitation scheme and energy levels.

The excitation schemes for both the oxygen transition and the CO transition is shown in Fig. 4. The oxygen atom transition excites from the $2p^3P_2$ ground state to the $3p^3P_{2,1,0}$ excited state at 225.6 nm and relaxes to the $3s^3S$ state with emission at 844.9 nm. This transition is a triplet state with three rotational levels spaced very close together. The CO excitation occurs from the $X^1\Sigma^+(v'' = 0)$ ground state to the $B^1\Sigma^+(v' = 0)$ state at 230 nm. The excited state emits

at 451 nm to the $A^1\Pi(v'' = 0)$ state, this is known as the (0,0) band. There are multiple closely spaced vibrational levels for emission so a narrow bandwidth filter is used to block these other wavelengths. The absorption wavelengths for both the oxygen atom and CO transitions are relatively close to each other. This has allowed for easy switching between probing both species thanks to the setup of the laser system.

The UVM Plasma Test and Diagnostics Laboratory (PTDL) is home to a Continuum Powerlite Nd:YAG (neodinium-doped yttrium aluminum garnet) laser as well as a Continuum ND6000 dye laser, as seen in Fig. 5. The Nd:YAG laser pumps 532nm light into the dye laser. The dye laser is able to produce a range of wavelengths ranging from 615 to greater than 655nm. Following the dye laser is a series of harmonic instruments which produce a final wavelength range between 224 to 230nm if the sum frequency mixing (SFM) method is used.

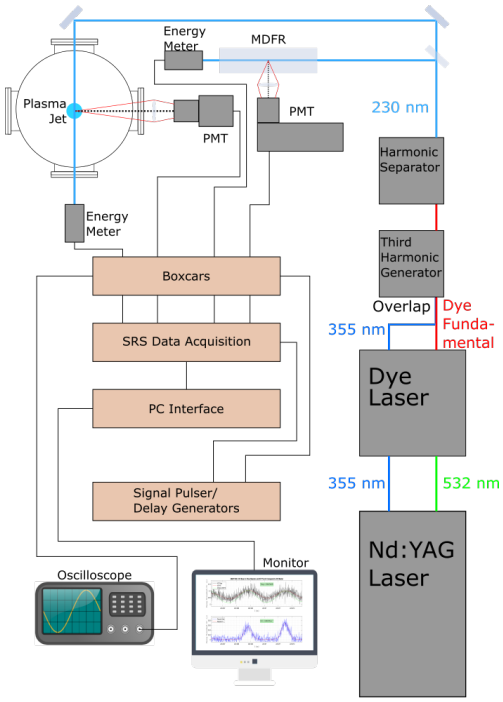

Fig. 5 General laser configuration used for sum frequency mixing.

This method was recently developed for generating UV light and allows for a greater range of tuning using a single dye, which makes changing between probing for oxygen atoms to CO extremely easy and fast. A change can now be done in minutes rather than days. Because of this both species can be probed during a single test [28]. For this method, 532nm light pumps the dye laser. 355nm light is extracted from the YAG using a third harmonic generator located inside the YAG. Both of these frequencies are extracted from the fundamental frequency which is 1064nm. The 355nm light bypasses the dye laser and is summed with the dye fundamental frequency before entering the third harmonic generator. A harmonic separator uses prisms to separate out each of the frequencies leaving UV light in the 224 to 230 nm range. An 80/20 beam splitter than splits the laser beam into two paths. The first of the paths reaches the Microwave Discharge Flow Reactor (MDFR) where baseline measurements are made with a photo-multiplier tube and energy meter. The second path is directed into the inductively coupled plasma chamber and through the plasma jet. Another photo-multiplier tube and energy meter takes measurements at this location.

A. TALIF Scan Improvements

A previous study of surface catalysis using oxygen atom and CO was done in the UVM ICP Facility but had limited success due to less than sufficient equipment available at the time [29]. A dual-grating installed in the dye laser has allowed for much more fine-tuning in scans and SFM allows for more resolution in transition structures that are close together in wavelength. A comparison between scans done previously and current scans are shown in Fig. 6. CO scans are especially improved as the individual rotational transitions are much more distinguishable than in the past.

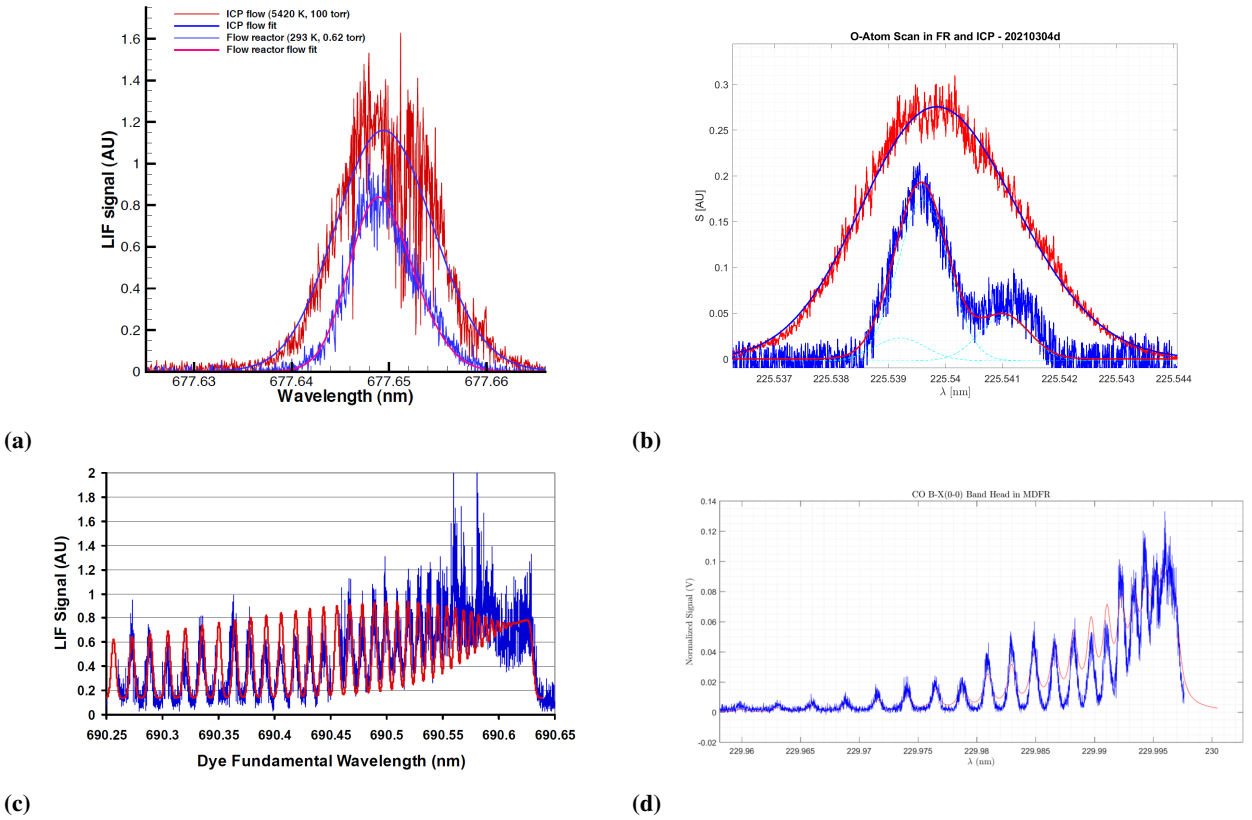

Fig. 6 a) Previous O-atom scan. b) Current O-atom scan. c) Previous CO bandhead scan. d) Current CO bandhead scan.

B. Temperature and Number Density Determination

A gaussian fit is implemented to each scan as collisional broadening is assumed to be negligible due to low pressures in the flow reactor and high temperatures in the ICP. If this was not the case a Lorentzian line shape would need to be accounted for and a Voigt fit would need to be implemented. These gaussian fits are shown in Fig. 6a and 6b, as well as Fig. 7.

Each scan is done at a different location over the sample surface. The laser is tuned over a wavelength range around the transition and scanned through the transition at a specified rate. As the wavelength passes through the transition and excites the atoms or molecules, the photo-multiplier tubes capture the emission from the fluorescence. Fig. 6b and Fig. 7 both show how the transitions broaden as temperature increases. The hyper-fine structure of the O-atom scan is distinguishable at low temperatures in the flow reactor but is not distinguishable at higher temperatures in the ICP. The broadening from temperature is known as Doppler broadening. The other mechanism causing broadening is the laser line width, which is the frequency span of the laser output. The two are related in that the square of the total spectral broadening contribution at each location is equal to the sum of the doppler broadening and laser line width each squared, since both are a gaussian shape. This occurs at the transition resonant wave number in the VUV [30].

$$(\Delta\hat{\nu}_{tot})^2 = (\Delta\hat{\nu}_D)^2 + 2(\Delta\hat{\nu}_{laser})^2 \tag{3}$$

Doppler broadening is derived from kinetic theory and can be described with Eq. 4:

$$\Delta\hat{\nu}_D = 7.162(10)^{-7}\hat{\nu}_0\sqrt{T/M} \tag{4}$$

where $\Delta\hat{\nu}_{tot}$ is the total line width, $\Delta\hat{\nu}_D$ is the doppler width, $\Delta\hat{\nu}_{laser}$ is the laser line width, $\hat{\nu}_0$ is the center wave number, T is temperature, and M is the molar mass. Relating Eq. 3 and 4 produces Eq. 5 in the ICP:

$$T_{ICP} = \frac{M}{(\hat{\nu}_0 7.162(10)^{-7})^2}\left[\left(\Delta\hat{\nu}_{tot,ICP}\right)^2 - \frac{\left((\Delta\hat{\nu}_{tot,FR})^2 - (\Delta\hat{\nu}_{D,FR})^2\right)}{2}\right] \tag{5}$$

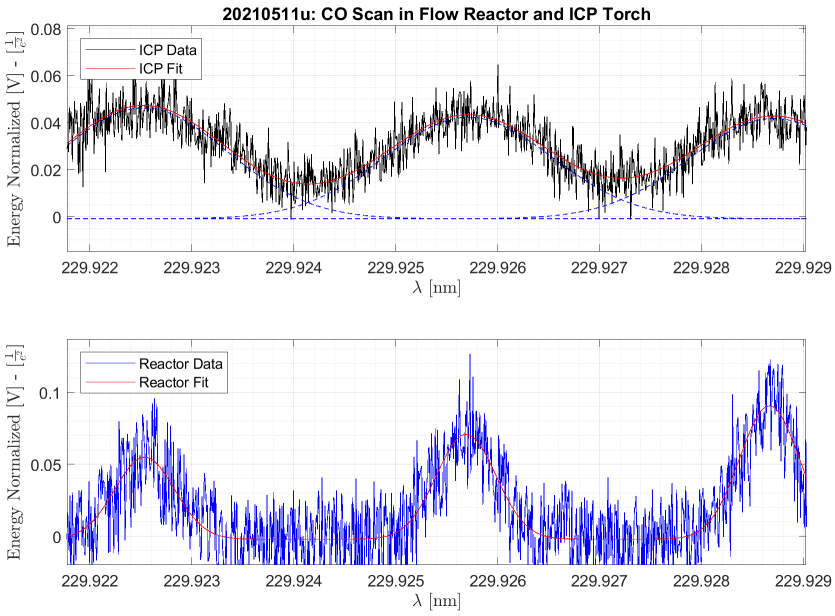

Fig. 7 CO B-X(0-0) scan based around J" = 20.

The relative number density is proportional to the spectral integral of the normalized LIF signal [31]:

$$n \propto \left(\int \frac{S_{LIF}}{E_p^2}(\lambda)d\lambda \times \frac{p}{T^{1/2}}\right) \times f_i(T)^{-1} = A \times f_i(T)^{-1} \tag{6}$$

where S_{LIF}/E_p^2 is the LIF signal normalized by the square of the laser energy and $p/T^{1/2}$ accounts for collisional quenching. $f_i(T)^{-1}$ is dependent on the species and is a temperature correction term as the population atoms or molecules in each state depend on the temperature. For O-atom the hyper-fine triplet ground-state must be corrected for and in CO there are a number of rotational states within the vibrational band that is being scanned through. The Boltzmann fraction is used to determine the temperature correction needed for the $J'' = 2$ transition in oxygen [32]:

$$f_O(T) = \left(\frac{5}{5 + 3e^{-228.75/T} + e^{-326.59/T}}\right) \tag{7}$$

as well as for the distribution of molecules among rotational energy levels for a heteronuclear molecule.

$$f_{CO}(T) = (2J+1)\,\frac{\theta_R}{T} exp\left(-J(J+1)\frac{\theta_R}{T}\right) \tag{8}$$

C. Catalytic Reaction Rate Coefficients

A summary on the steps required to determine the catalytic reaction rate efficiency is described, with further details found in [33].

The approach follows Goulard's mass balance at a catalytic wall [34]. First, the sample surface needs to be found. This is done using the ratio of beam energies measured with molectrons located after the flow reactor and ICP. Beam clipping is apparent when the ratio begins to drop suddenly, as seen in Fig. 8, done during a CO boundary layer survey. A linear fit is implemented over the clipped data points. The 50% value between no clipping and 0 (fully blocked)

is determined to be where the sample surface is located. Twice the distance from the sample surface to the onset of blocking is determined to be the beam diameter. O-atom scans had a beam diameter of 1.2 mm and CO scans had a beam diameter of 0.8 mm.

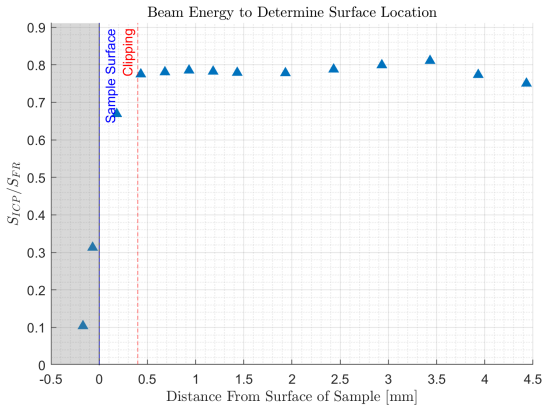

Fig. 8 Method for determining where the sample surface is located using beam energy.

A temperature fit is implemented due to the large uncertainty in the temperature measurements. The catalytic reaction rate efficiency is ultimately calculated using the fit temperatures rather than the measured temperatures. The fit used is a two-component exponential growth model seen in Eq. 9. This model is not physical but provides a good fit to the temperature trend:

$$T = T_{surf} + B_1\left(1 - exp\left(\frac{-y}{B_2}\right)\right) + B_3\left(1 - exp\left(\frac{-y}{B_4}\right)\right) \tag{9}$$

where B_i represents the fit parameters. From the temperature fit, the number density distribution can be calculated:

$$n_{fit}(y) = \frac{p_{static}}{k_B T_{fit}(y)} \tag{10}$$

where p_{static} is the chamber pressure and k_B is the Boltzmann constant ($1.3806 \times 10^{-23} m^2 \cdot kg \cdot s^{-2} \cdot J \cdot K^{-1}$).

The relative atom or molecular mole fraction is found from the integrated area, temperature fit, and number density distribution. It is normalized by free-stream conditions at approximately 3 mm from the sample surface.

$$\hat{\chi_i}(y) = \frac{A \times f_i(T)^{-1}/n_{fit}(y)}{A(3mm) \times f_i(T)^{-1}/n_{fit}(3mm)} \tag{11}$$

A diffusion coefficient is needed to determine how O and CO interact with each other [33]:

$$D = D_0\left(\frac{p_0}{p}\right)\left(\frac{T}{T_0}\right)^{1.841} \tag{12}$$

where $D_0 = 0.27 cm^2 \cdot s^{-1}$ at reference conditions of 298 K and 760 Torr [35]. This diffusion coefficient is for a Oxygen Argon mixture, which is similar to the mixture of this work, but there has not been success in finding a diffusion coefficient for an O-CO or CO-O mixture which consists of two polar species diffusing through each other.

A surface reaction rate can now be determined:

$$k_w = \frac{D_{iw}}{\hat{\chi_{iw}}}\left(\frac{\partial_{\hat{\chi_i}}}{\partial_y}\right)_w \tag{13}$$

where D_{iw} is the diffusion coefficient at the wall, $\hat{\chi_{iw}}$ is the relative specie mole fraction at the wall, and $(\partial_{\hat{\chi_i}}/\partial_y)$ is the near-wall relative atom or molecular mole fraction gradient.

Finally, the catalyzed reaction efficiency can be determined which represents the ratio of atoms recombined at the surface to the number arriving:

$$\gamma_i = \frac{k_{wi}}{\sqrt{RT_w/2\pi M_i}} \tag{14}$$

where R is the universal gas constant ($8.3144598 J \cdot K^{-1} \cdot mol^{-1}$) and M_i is the molar mass ($kg \cdot mol^{-1}$).

IV. Results

A. Previous Results

The UVM ICP Facility previously undertook boundary layer surveys over a cooled copper surface using oxygen atom and CO scans [29]. As described earlier, there were limitations from equipment at the time of these tests, and various improvements such as a dual grating in the dye laser and the SFM method have been implemented since this test campaign.

It is shown in Fig. 9 that there were a limited number of scans performed for the survey, especially for CO. The temperature measurements do, however, match well. The oxygen atom relative number density suggests that molecular oxygen recombination is occurring close to the surface. CO_2 recombination does not appear to be occurring based on this data, as the relative number density does not show a trend in any one direction.

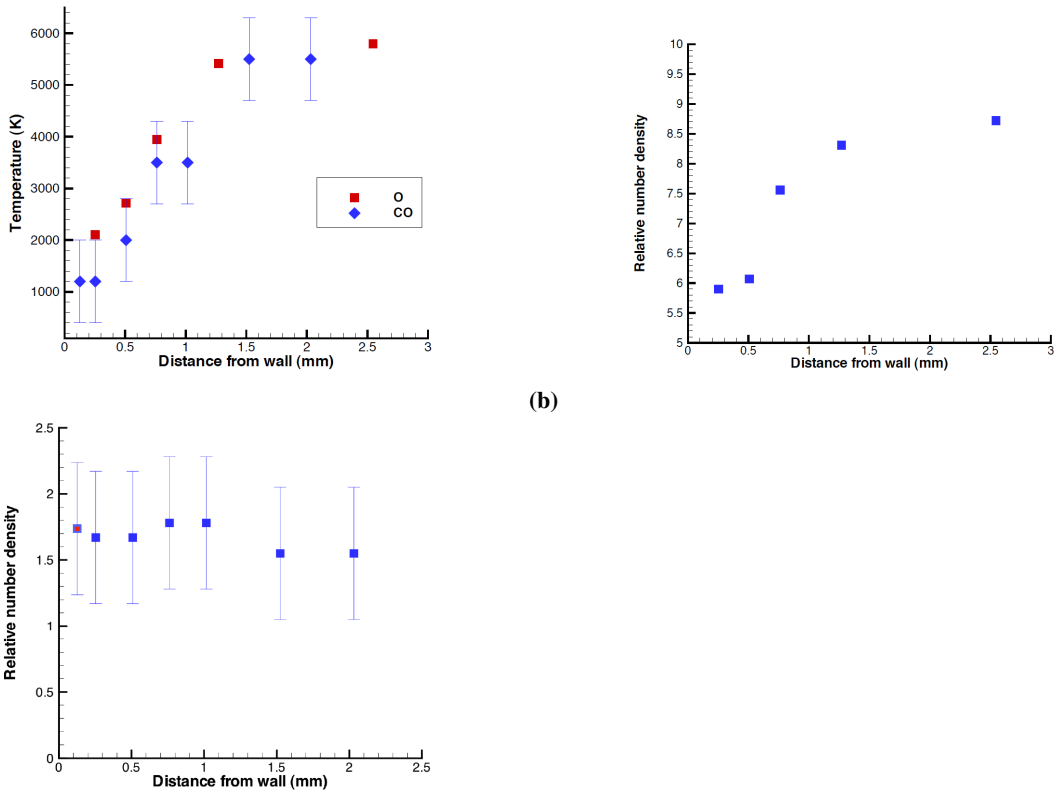

Fig. 9 a) Previous temperature measurements of oxygen atom and CO over a water cooled copper sample. b) Previous oxygen atom relative number density measurements over a water cooled copper sample. c) Previous CO relative number density measurements over a water cooled copper sample.

B. Radial Free Stream Temperature Survey

Before boundary layer scans could be done, a reliable method for CO temperature scans needed to be obtained. CO scans had not been done using the SFM method up to this point, so new code needed to be written to produce

temperatures that should agree with O-atom temperatures. O-atom is considered to be a reliable method of temperature measurement as it has been utilized many times with the same SFM method, and has produced consistent results over time.

A series of free stream radial temperature scans were conducted and are shown in Fig. 10. The objective of these tests were to produce repeatable measurements that agreed with the accepted O-atom measurements, as well as to determine an optimal Argon-CO_2 mixture. Argon is an inert gas that does not react with any of the other species in the flow. It also acts as a good coupler allowing the facility to operate in a stable condition and for a longer period of time.

Measurements were made at the center of the plasma jet, the edge of the plasma jet, and various points in between. The center of the jet should be the hottest and the edge should be the coolest.

Fig. 10a shows multiple scans performed on different days and with different gas mixtures, whereas Fig. 10b, 10c, and 10d show scans done with only the same gas mixture. This is important because different mixtures will produce different temperatures. Because Argon is a good coupler, it produces a high temperature plasma compared to CO_2. The more Argon in the flow, the hotter the overall plasma should be. Also, the facility runs different on some days compared to others. Over time, general conditions of the facility will change and could produce slightly different temperatures even when all the variables are held the same. The laser line width contribution to the line broadening causes a large uncertainty in temperature measurements of about ± 500 K [33].

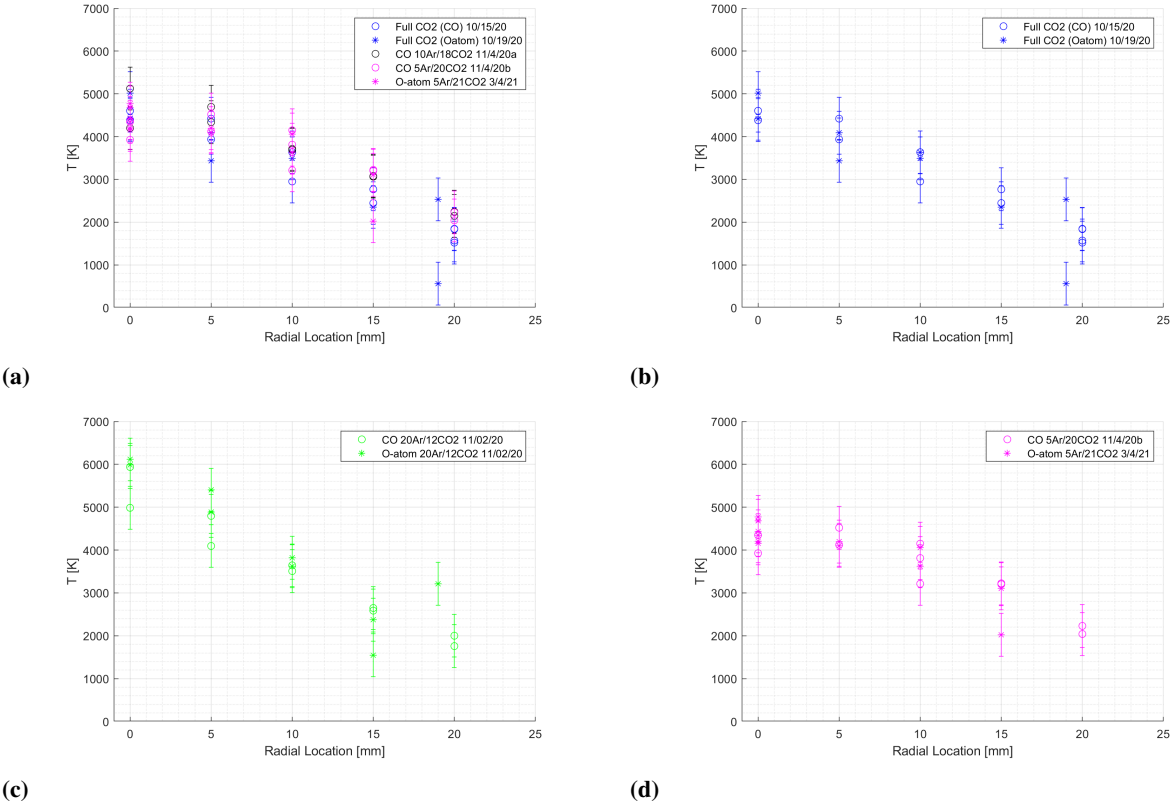

Fig. 10 Radial temperatures in a CO_2 plasma. a) Varying Mixtures b) 23 slpm CO_2 c) 12 slpm CO_2 / 20 slpm Ar d) 21 slpm CO2 / 5 slpm Ar

With these uncertainties taken into account, the temperature values measured for both O-atom and CO match reasonably well. High temperatures at the center of the jet trend downwards towards the edge, as expected. A higher Argon mixture case also produced higher temperatures.

From these various testing cases, an ideal gas mixture was also determined, which was a qualitative decision. While performing these tests, it was found that on average a mixture of about 5 slpm Argon and 21 slpm CO_2 was an ideal case because it generally produced longer run times in the facility and also made detecting the CO B-X transition and O-atom transition easier, as Argon caused background noise that made it difficult to see the signal in the ICP. With

confidence in temperature measurements, catalytic boundary condition scans are possible.

C. Boundary Layer Survey Over Water-Cooled Copper

Boundary layer surveys consist of taking TALIF scans at various points in front of a sample surface. For this work, a survey was taken ahead of a water cooled copper sample. Copper is known to be a catalytic material that allows for the $O + O \rightarrow O_2$ reaction. Temperature and relative number density measurements for both O-atom and CO are shown in Fig. 11. The shaded grey region represents the sample surface, the blue dotted line represents the onset of beam clipping during the O-atom scans and the dotted red line represents the onset of beam clipping during the CO scans. Temperature measurements for both O-atom and CO match well and show a decreasing temperature towards the surface of the sample, as expected. Temperature values begin to level out as measurements move out of the boundary layer and into the free stream. The relative number densities were normalized to one so that the trends could be compared to each other. Relative number density measurements for O-atom show that O_2 recombination is likely occurring, as the number density of O is decreasing towards the surface. The jump in number density for both O-atom and CO measurements ahead of the clipping is expected and indicates non-catalytic behaviour right above the surface. CO exhibits a fairly constant number density throughout most of the boundary layer. This suggests that CO_2 recombination is a slow reaction. The overall number density of the gas mixture will increase as temperature decreases while pressure remains constant. The slight rise in CO number density towards the surface is likely a result of this.

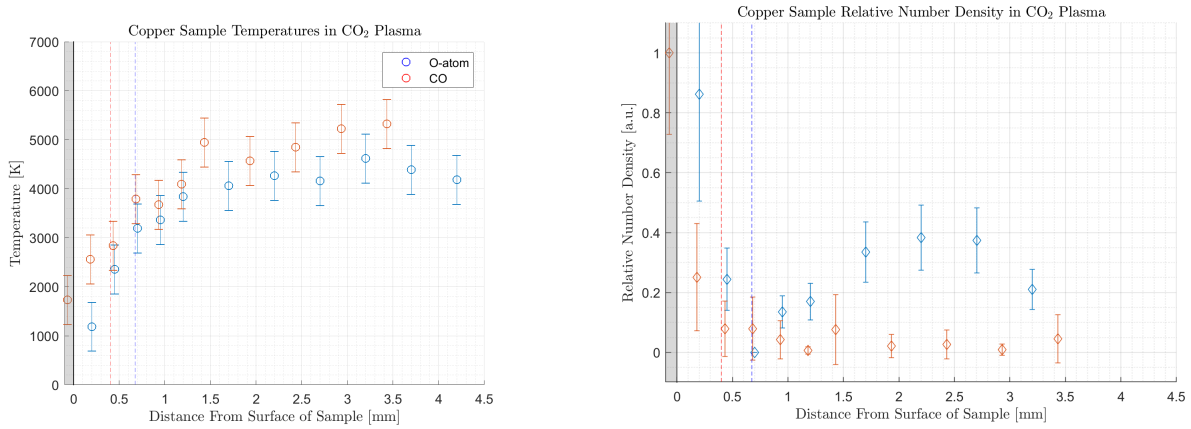

(a) **(b)**

Fig. 11 a) Boundary layer temperature scans over a water-cooled copper sample with CO and O-atom. b) Boundary layer relative number density scans over a water-cooled copper sample with CO and O-atom.

Fig. 12 and 14 show the general approach for determining the surface catalyzed recombination efficiencies for O-atom and CO, respectively. The temperature fit is seen on the upper left and indicates the sample surface temperature and free stream temperature. The sample surface temperature is an estimated value based on the trend of the temperatures. In future measurements, a two-color pyrometer or IR camera will be used to directly measure the surface temperature. The fit lines follow the temperature values well and red dots indicate the wall temperature and free stream temperature. The upper right shows the relative number density individually for a more clear view. The lower left shows the number density from the temperature fit described by Eq. 10. The lower right shows the relative atom mole fraction with a linear fit to determine the near-wall relative atom mole fraction gradient. The fit is constrained to within 1 mm which is within the boundary layer. Fig. 13 shows the relative mole fraction near the sample wall. O-atom shows a positive slope indicating recombination near the surface and CO shows a zero gradient slope indicating no recombination.

Table 2 shows relevant data from the measurements. The catalytic efficiency of O-atom was found to be 0.0274 ± 0.009 and the catalytic efficiency of CO was found to be 0 ± 0.0004. This indicates a stronger O_2 recombination model than CO_2 recombination.

Table 2 O-atom and CO relevant data.

Species	T_{surf}, K	T_{edge}, K	$(\partial_{\hat{\chi}_i}/\partial_y)_w, mm^{-1}$	$\hat{\chi}_{iw}$	$D_{iw}, cm^2/s$	$k_w, m/s$	γ_i
O-atom	600	4500	0.344	0.2837	4.65	6.10	0.0274 ± 0.00090
CO	2000	5700	0	0.710	4.65	0	0 ± 0.0004

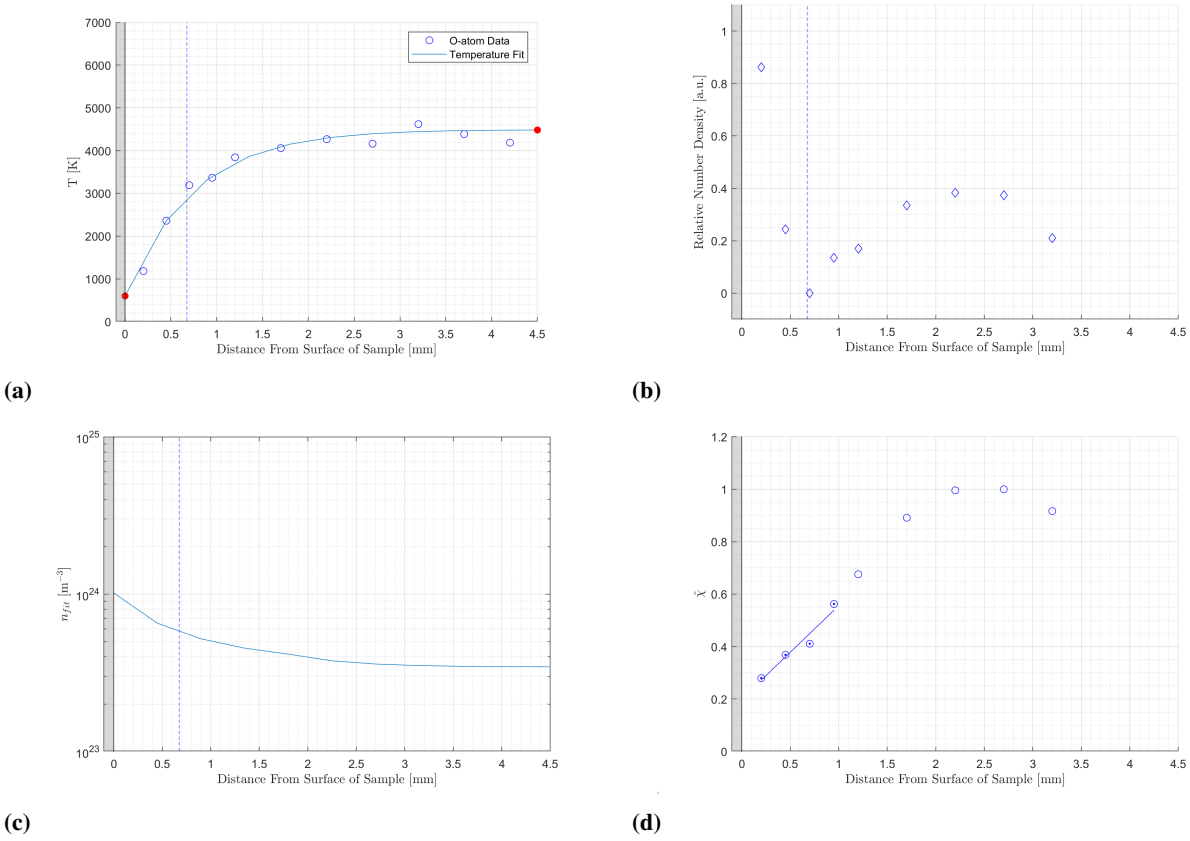

(a) **(b)**

(c) **(d)**

Fig. 12 Water-cooled copper O atom measurements in a CO_2 plasma. a) Temperature and fit. b) Number density from normalized integrated area. c) Number density from temperature fit. d) Near-wall linear fit of relative atom mole fraction.

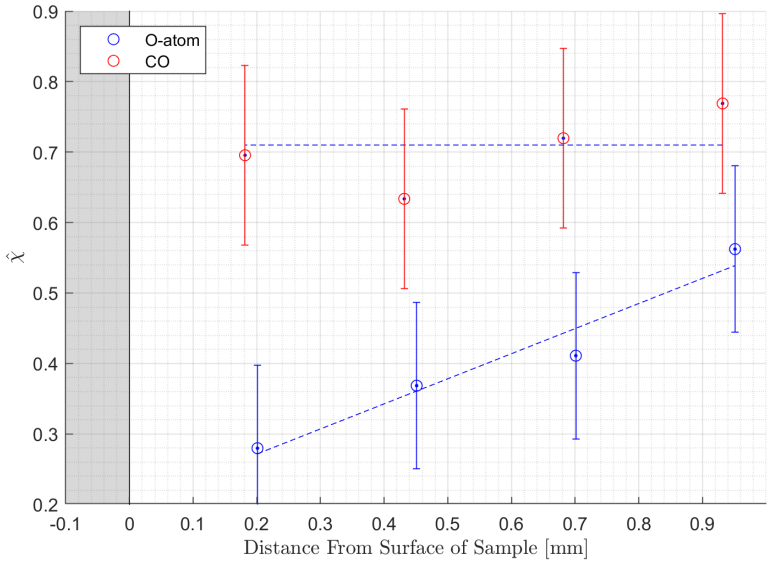

Fig. 13 Normalized near-surface relative mole fraction for O-atom and CO on water-cooled copper sample.

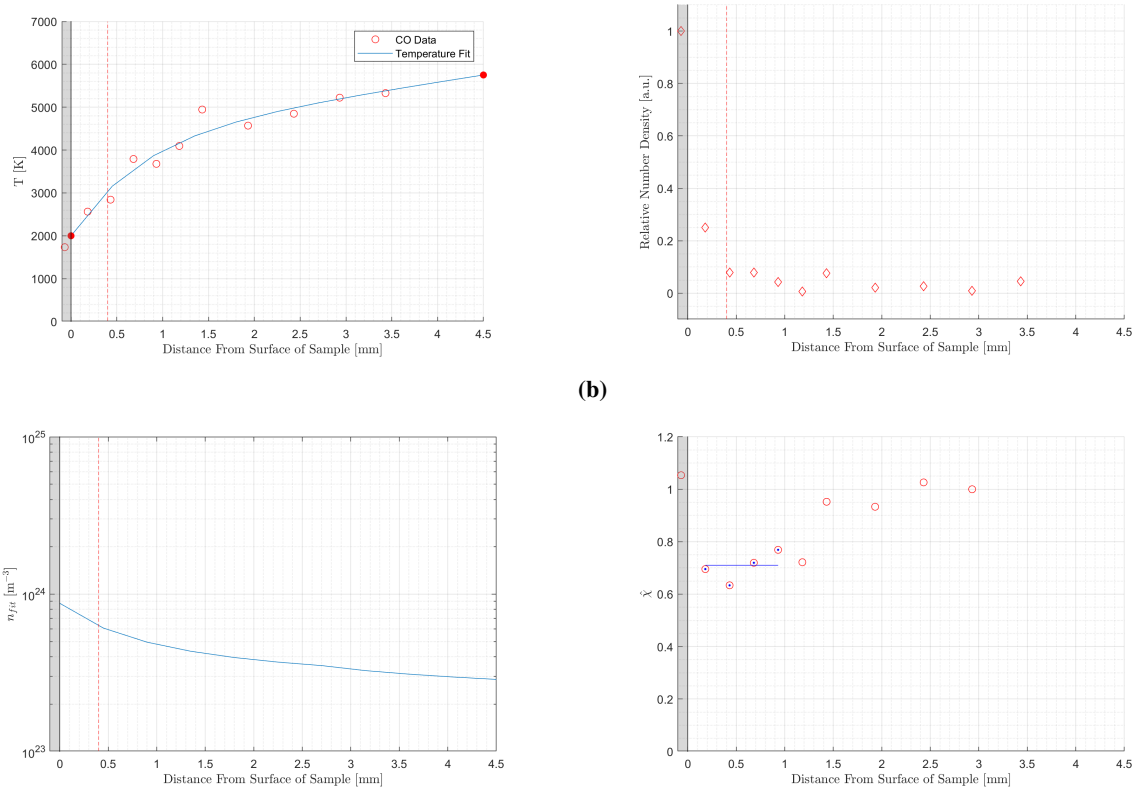

Fig. 14 Water-cooled copper CO measurements in a CO_2 plasma. a) Temperature and fit. b) Number density from normalized integrated area. c) Number density from temperature fit. d) Near-wall linear fit of relative molecular mole fraction.

V. Conclusion

This work used spatially resolved TALIF measurements to determine the surface catalytic efficiency of molecular oxygen and carbon dioxide recombination reactions above a water cooled copper sample in a predominantly CO_2 plasma simulating Martian atmospheric entry.

Results indicate that O_2 recombination is the dominant recombination reaction occurring near the surface of the sample while CO_2 recombination is minimal. This supports Sepka's model of a dominant O_2 recombination environment which has been the more prevalent model recently. A super-catalytic boundary condition is not supported with these findings and instead a partially-catalytic model would be supported. This would mean that TPS has been overbuilt in the past and available payload has been lost to unnecessary heat shied mass. These results may aid in the development of TPS with a more optimal mass design.

A. Future Work

This work was a first attempt at determining boundary layer conditions in a CO_2 plasma while probing both O-atoms and CO molecules with recent upgrades to the UVM facility. To progress further, more boundary layer scans will be done over varying catalytic surfaces with higher spatial resolution. Direct measurements of the surface temperature will also provide more accurate results. A diffusion coefficient for O-CO and CO-O will also utilized at such time as it is found in literature and will replace the current use of an O-Ar diffusion coefficient mixture where it is assumed that the value of the coefficients is similar.

Acknowledgments

This work was supported by NASA EPSCoR award 17-EPSCoRProp-0042, Scott Splinter (NASA LRC) and Michael Wright (NASA ARC), technical monitors.

References

[1] Anderson, J. D., *Modern Compressible Flow with Historical Perspective*, 3rd ed., MCGRAW-HILL US HIGHER ED, India, 2020, Chap. 15.

[2] Dutta, S., and Braun, R. D., "Statistical Entry, Descent, and Landing Performance Reconstruction of the Mars Science Laboratory," *Journal of Spacecraft and Rockets*, Vol. 51, No. 4, 2014, pp. 1048, 1061. https://doi.org/10.2514/1.a32937.

[3] Holstein-Rathlou, C., Maue, A., and Withers, P., "Atmospheric Studies from the Mars Science Laboratory Entry, Descent and Landing Atmospheric Structure Reconstruction," *Planetary and Space Science*, Vol. 120, 2016, pp. 15, 23. https://doi.org/10.1016/j.pss.2015.10.015.

[4] Little, A., Bose, D., Kaarlgard, C., Munk, M., Kuhl, C. A., Schoenenberger, M., Antill, C., Verhappen, R., Kutty, P., and White, T., "The Mars Science Laboratory (MSL) entry, descent and landing instrumentation (MEDLI): hardware performance and data reconstruction," *36th AAS Guidance and Control Conference*, NASA, Breckenridge, CO, 2013.

[5] Wright, M., Edquist, K., Tang, C., Hollis, B., Krasa, P., and Campbell, C., "A Review of Aerothermal Modeling for Mars Entry Missions," *48th AIAA Aerospace Sciences Meeting Including the New Horizons Forum and Aerospace Exposition*, AIAA, Orlando, Florid, 2010.

[6] Gordon, S., and McBride, B. J., "Computer Program for Calculation of Complex Chemical Equilibrium Compositions and Applications," *NASA Reference Publication 1311*, NASA, 1996.

[7] Meyers, J. M., Owens, W. P., Dougherty, M., Lutz, A., Uhl, J., and Fletcher, D. G., "Laser Spectroscopic Investigation of Surface-Catalyzed Reactions for Mars Exploration Vehicles," *27th AIAA Aerodynamic Measurement Technology and Ground Testing Conference*, American Institute of Aeronautics and Astronautics, Chicago, Illinois, 2012.

[8] Chen, Y.-K., Henline, W. D., Stewart, D. A., and Candler, G. V., "Navier-Stokes Solutions with Surface Catalysis for Martian Atmospheric Entry," *Journal of Spacecraft and Rockets*, Vol. 30, No. 1, 1993, pp. 32, 42. https://doi.org/10.2514/3.25468.

[9] Mitcheltree, R. A., "Computational Aerothermodynamics for Mars Pathfinder Including Turbulence," AIAA Paper No. 95-3493, Aug. 1995.

[10] Sepka, S., Chen, Y.-K., Marschall, J., and Copeland, R. A., "Experimental Investigation of Surface Reactions in Carbon Monoxide and Oxygen Mixtures," *Journal of Thermophysics and Heat Transfer*, Vol. 14, No. 1, 2000, pp. 45, 52. https://doi.org/10.2514/2.6488.

[11] Kolesnikov, A. F., Pershin, I. S., Vasil'evskii, S. A., and Yakushin, M. I., "Study of Quartz Surface Catalycity in Dissociated Carbon Dioxide Subsonic Flows," *Journal of Spacecraft and Rockets*, Vol. 37, No. 5, 2000, pp. 573, 579. https://doi.org/10.2514/2.3629.

[12] MacLean, M., Wadhams, T., Holden, M., and Hollis, B., "Investigation of Blunt Bodies with CO2 Test Gas Including Catalytic Effects," AIAA Paper No. 2005-4693, Jun. 2005.

[13] MacLean, M., Wadhams, T., and Holden, M., "Catalytic Effects on Heat Transfer Measurements for Aerothermal Studies with CO2," AIAA Paper No. 2006-0182, Jan. 2006.

[14] Wright, M. J., Olejniczak, J., Brown, J. L., Hornung, H., and Edquiest, K. T., "Modeling of Shock Tunnel Aeroheating Data on the Mars Science Laboratory Aeroshell," *Journal of Thermophysics and Heat Transfer*, Vol. 20, No. 4, 2006, pp. 641, 651. https://doi.org/10.2514/1.19896.

[15] Marschall, J., Copeland, R., Hwang, H., and Wright, M., "Surface Catalysis Experiments on Metal Surfaces in Oxygen and Carbon Monoxide Mixtures," *44th AIAA Aerospace Sciences Meeting and Exhibit*, AIAA, Reno, Nevada, Jan. 2006.

[16] Gnoffo, P. A., "A Perspective on Computational Aerothermodynamics at NASA," *16th Australasian Fluid Mechanics Conference*, NASA Langley Research Center, Crown Plaza, Gold Coast, Australia, 2007.

[17] Edquist, K., Dyakonov, A., Wright, M., and Tang, C., "Aerothermodynamic Design of the Mars Science Laboratory Heatshield," *41st AIAA Thermophysics Conference*, AIAA, San Antonio, Texas, 2009.

[18] Maclean, M., Marineau, E., Parker, R., Dufrene, A., Holden, M., and DesJardin, P., "Effect of Surface Catalysis on Measured Heat Transfer in Expansion Tunnel Facility," *Journal of Spacecraft and Rockets*, Vol. 50, No. 2, 2013, pp. 470, 475. https://doi.org/10.2514/1.A32327.

[19] Hollis, B. R., Prabhu, D. K., MacLean, M., and Dufrene, A., "Blunt-Body Aerothermodynamic Database from High-Enthalpy Carbon-Dioxide Testing in an Expansion Tunnel," *Journal of Thermophysics and Heat Transfer*, Vol. 31, No. 3, 2017, pp. 712, 731. https://doi.org/10.2514/1.T5019.

[20] Owens, W., Uhl, J., Dougherty, M., Lutz, A., Fletcher, D., and Meyers, J., "Development of a 30kW Inductively Coupled Plasma Torch for Aerospace Material Testing," *10th AIAA/ASME Joint Thermophysics and Heat Transfer Conference*, AIAA, Chicago, Illinois, 2010.

[21] Kolesnikov, A. F., "Conditions of Simulation of Stagnation Point Heat Transfer from a High-Enthalpy Flow," *Fluid Dynamics*, Vol. 28, No. 1, 1993, pp. 131, 137. https://doi.org/10.1007/BF01055676.

[22] Kwak, H. S., Uhm, H. S., Hong, Y. C., and Choi, E. H., "Disintegration of Carbon Dioxide Molecules in a Microwave Plasma Torch," *Sci. Rep.*, 5, 18436, 2015. https://doi.org/10.1038/srep18436.

[23] Tango, W. J., Link, J. K., and Zare, R. N., "Spectroscopy of K_2 Using Laser-Induced Fluorescence," *The Journal of Chemical Physics*, Vol. 49, No. 10, 1968, pp. 4264, 4268. https://doi.org/10.1063/1.1669869.

[24] Bamford, D. J., Jusinski, L. E., and Bischel, W. K., "Absolute two-photon absorption and three-photon ionization cross sections for atomic oxygen," *Phys. Rev. A*, Vol. 34, No. 1, 1986, pp. 185, 198. https://doi.org/10.1103/PhysRevA.34.185.

[25] Loge, G. W., Tiee, J. J., and Wampler, F. B., "Multiphoton-Induced Fluorescence and Ionization of ($B^1\Sigma^+$) Carbon Monoxide," *The Journal of Chemical Physics*, Vol. 79, No. 1, 1983, pp. 196, 202. https://doi.org/10.1063/1.445556.

[26] Aldén, M., Wallin, S., and Wendt, W., "Applications of two-photon absorption for detection of CO in combustion gases," *Applied Physics B*, Vol. 33, 1984, pp. 205, 208. https://doi.org/10.1007/BF00697329.

[27] Di Rosa, M., and Farrow, R., "Cross sections of photoionization and Stark shift for 2 + 1 REMPI of CO," *AIAA 1998-2477. 29th AIAA, Plasmadynamics and Lasers Conference*, Albuquerque, NM, 1998.

[28] Herrmann-Stanzel, R., "Energy Accommodation from Surface Catalyzed Reactions in Air Plasmas," *Graduate College Dissertations and Theses*, 1012. 2019. URL https://scholarworks.uvm.edu/graddis/1012.

[29] Dougherty, M., Owens, W., Meyers, J., and Fletcher, D., "Investigations of Surface-Catalyzed Recombination Reactions in the Mars Atmosphere," *AIAA 2011-1326. 49th AIAA Aerospace Sciences Meeting including the New Horizons Forum and Aerospace Exposition*, Orlando, Florida, January 2011.

[30] Fletcher, D. G., "Arcjet Flow Properties Determined from Fluorescence of Atomic Nitrogen," *Applied Optics*, Vol. 38, No. 9, 1999, pp. 1850, 1858. https://doi.org/10.1364/AO.38.001850.

[31] Fletcher, D. G., Thömel, J., Chazot, O., and Marschall, J., "Realization of a Gas–Surface Interaction Test Case for Model Validation," *48th AIAA Aerospace Sciences Meeting*, AIAA Paper 2010-1249, Jan. 2010.

[32] Vincenti, W. G., and Kruger, C. H., *Introduction to Physical Gas Dynamics*, Wiley, New York, 1967, p. 131.

[33] Fletcher, D. G., and Meyers, J. M., "Surface Catalyzed Reaction Efficiencies in Oxygen Plasmas from Laser-Induced Fluorescence Measurements," *Journal of Thermophysics and Heat Transfer*, Vol. 31, No. 2, 2017, pp. 410, 420. https://doi.org/10.2514/1.T4923.

[34] Goulard, R., "On Catalytic Recombination Rates in Hypersonic Stagnation Heat Transfer," *Journal of Jet Propulsion*, Vol. 28, No. 11, 1958, pp. 737, 745. https://doi.org/10.2514/8.7444.

[35] Marrero, T. R., and Mason, E. A., "Gaseous Diffusion Coefficients," *Journal of Physical Chemistry Reference Data*, Vol. 1, No. 1, 1972, pp. 3, 118. https://doi.org/10.1063/1.3253094.